kinds of cells in bone. Although adiponectin was confirmed not to be expressed in the Ad−/− cells, AdipoR1, and AdipoR2 were detected in both osteoblasts and osteoclasts. In addition, all were also detected in a mouse stromal cell line ST2. These results indicate that adiponectin acts on bone not only through an endocrine pathway as a hormone secreted from fat tissue, but also through an autocrine/paracrine pathway. To elucidate the actions of adiponectin through these distinct pathways, we next performed experiments using the deficient and overexpressing transgenic mice.

No Abnormality in Bone of Adiponectin-Deficient Mice In Vivo

To examine the role of endogenous adiponectin in bone metabolism, we analyzed the bones of Ad−/− mice. Ad−/− mice developed and grew normally, indicating that adiponectin is not involved in the regulation of skeletal growth. X-ray analyses showed no significant difference in the skeleton between Ad−/− and WT littermates at 8 weeks of age (Fig. 2A). BMDs of the entire femurs, tibiae, and vertebrae (L2-L5) were also similar between mice of the two genotypes (Fig. 2B). In accordance with X-ray and BMD findings, histological analyses of the proximal tibiae of 8-week-old Ad−/− mice by the Villanueva–Goldner staining revealed no difference in bone phenotypes from those of WT littermates (Fig. 2C). The growth plate at the proximal tibiae of Ad−/− mice also seemed similar to that of WT, consistent with the lack of contribution of adiponectin to the skeletal growth. Bone histomorphometric measurements in this area supported these histological observations (Table I): there was no difference between Ad−/− and WT littermates in bone volume (BV/TV), bone formation parameters (Ob.S/BS & BFR), or bone resorption parameters (Oc.S/BS & ES/BS).

Suppression of Osteogenesis in the Culture of Adiponectin-Deficient Bone Marrow Cells

Considering that adiponectin acts through both endocrine and autocrine/paracrine pathways, the lack of abnormal phenotype in the bones of Ad−/− mice, which are not bone-specific conditional knockout mice but conventional knockout mice, may possibly be due to the equivalent balance of the two pathways. To examine the specific effect of the autocrine/paracrine action of adiponectin, in vitro cultures of bone marrow cells from Ad−/− and WT mice were compared. Surprisingly, osteogenesis determined by the number of colonies positively stained with ALP and Alizarin red was significantly decreased in the Ad−/− marrow cell culture as compared with that in the WT culture, suggesting a positive effect of the autocrine/paracrine action on bone formation (Fig. 3A, left and middle panels). However,

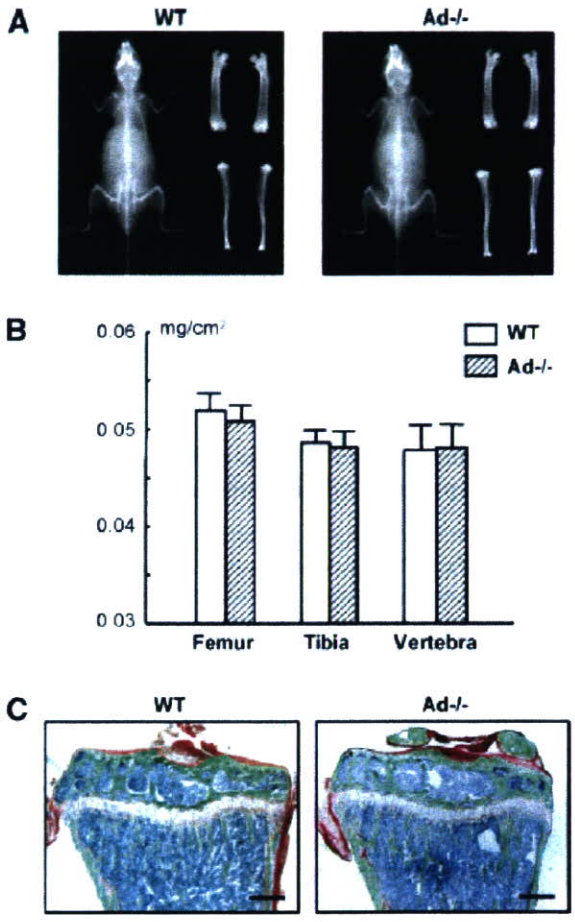

Fig. 2. Radiological and histological findings of the bones in male WT and Ad−/− littermates (8 weeks old). **A**: Plain X-ray images of the whole bodies (**left**), femurs (**upper right**), and tibiae (**lower right**) of representative WT and Ad−/− littermates. **B**: BMD of the entire femurs, tibiae, and L2-L5 vertebral bodies determined by DEXA. Data are expressed as means (bars) ± SEM (error bars) of 10 bones/group. None of the bones showed significant difference of BMD between the two genotypes. **C**: Histological features of the proximal tibiae of representative mice of each genotype. After the sacrifice, the tibiae were excised, fixed, embedded without decalcification, and the sagittal sections were stained with Villanueva–Goldner, in which mineralized bone was stained green and unmineralized osteoid red. Bar, 100 μm. Data of histomorphometric analyses are shown in Table I. [Color figure can be viewed in the online issue, which is available at www.interscience.wiley.com.]

TABLE I. Histomorphometry of Trabecular Bones in Proximal Tibiae of WT and Ad−/−Mice

	BV/TV (%)	Ob.S/BS (%)	BFR (mm^3/cm^2/year)	Oc.S/BS (%)	ES/BS (%)
WT	12.75 ± 0.96	11.93 ± 0.90	3.66 ± 0.92	4.58 ± 1.78	3.52 ± 0.79
Ad−/−	10.71 ± 1.92	12.07 ± 1.22	3.16 ± 0.93	4.32 ± 1.38	3.82 ± 0.89

Parameters for the trabecular bone were measured in an area 1.2 mm in length from 250 μm below the growth plate at the proximal metaphysis of the tibiae in Villanueva–Goldner and calcein double-labeled sections. Data expressed as means and standard errors (SEM) for 10 bones/group.
No significant difference of parameters between two genotypes (all $P > 0.05$).
BV/TV, trabecular bone volume expressed as a percentage of total tissue volume; Ob.S/BS, percentage of bone surface covered by cuboidal osteoblasts; BFR, bone formation rate; Oc.S/BS, percentage of bone surface covered by mature osteoclasts; ES/BS, percentage of eroded surface.

adipogenesis determined by the oil red O staining in the marrow cell culture was similar between Ad−/− and WT marrow cell cultures (Fig. 3A; right panel). To investigate the role of local adiponectin in osteoclastic cells, we next measured the number of TRAP-positive multinucleated osteoclasts formed in the coculture of bone marrow cells and primary osteoblasts, and found no difference between the cells of the two genotypes (Fig. 3B).

No Abnormality in Bone of Transgenic Mice Overexpressing Adiponectin in the Liver In Vivo

The in vivo Ad−/− bone analyses showed the equivalent balance of autocrine/paracrine and endocrine actions of adiponectin on bone (Fig. 2), while the in vitro Ad−/− marrow culture revealed the positive autocrine/paracrine action on bone formation (Fig. 3). These results imply a negative effect of circulating adiponectin on bone formation. Hence, we next examined the skeletal abnormality of transgenic mice overexpressing adiponectin (Ad-Tg) being driven by the SAP promoter, so that the adiponectin expression was limited to the liver and was not in the bone [Yamauchi et al., 2003b]. Ad-Tg mice appeared normal and indistinguishable from WT littermates in body weight and length. Plain X-ray images of Ad-Tg mice at 8 weeks showed no abnormality in the skeleton compared with WT littermates (Fig. 4A), and BMDs of the entire femurs, tibiae, and vertebrae (L2-L5) of Ad-Tg mice were also similar to those of WT littermates (Fig. 4B). Histological analyses of the proximal tibiae by the Villanueva–Goldner staining (Fig. 4C) and bone histomorphometric measurements (Table II) confirmed that neither the bone mass nor the bone turnover was affected by the circulating adiponectin.

Suppression of Osteogenesis by Recombinant Adiponectin in Osteoprogenitor Cell Cultures

We failed to detect the expected negative effect of circulating adiponectin on bone formation in Ad-Tg mice in vivo. However, since adiponectin is known to enhance the insulin action on its target organs [Berg et al., 2001; Combs et al., 2001; Fruebis et al., 2001; Yamauchi et al., 2001, 2003b; Kubota et al., 2002], the effect of circulating adiponectin on bone might partly be mediated by the insulin signaling that is anabolic for bone formation [Thomas et al., 1996]. Hence, we next looked at the systemic (or endocrine) action by examining the effect of addition of recombinant adiponectin on osteogenesis in cultures of osteoprogenitor cells in the presence and absence of insulin. In the cultures of bone marrow cells derived from WT long bones, osteogenesis determined by the numbers of colonies positively stained with ALP and Alizarin red were dose-dependently inhibited by recombinant adiponectin in the absence of insulin, indicating a direct/negative action of adiponectin on bone formation (Fig. 5A). However, in the presence of insulin (10 nM), the inhibition of osteogenesis by adiponectin was not seen in either ALP or Alizarin red staining. In the culture of mouse stromal cell line ST2, recombinant adiponectin also did not decrease ALP activity which was stimulated by IGF-I (100 nM), another bone anabolic factor that shares downstream molecules with the insulin signaling (Fig. 5B). In contrast, it dose-dependently decreased ALP activity which was stimulated by BMP-2 (10 nM).

We then investigated the effect of adiponectin on the intracellular signaling of insulin in bone marrow cells by examining the phosphorylations

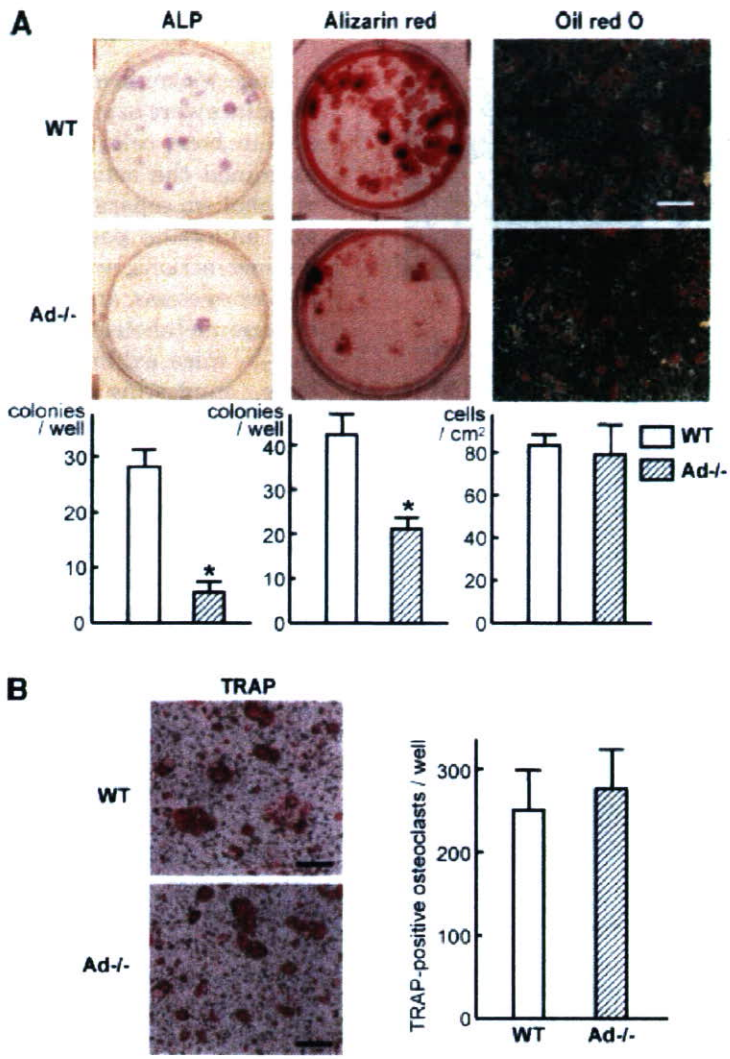

Fig. 3. Osteogenesis, adipogenesis, and osteoclastogenesis in cultures of bone marrow cells from WT and Ad−/− littermates. **A**: Osteogenesis was determined by ALP (**left**) and Alizarin red (**middle**) stainings of bone marrow cells cultured for 10 and 21 days, respectively, in αMEM/10% FBS with ascorbic acid and β-glycerophosphate. Adipogenesis was determined by oil red O staining (**right**) of bone marrow cells cultured for 10 days in αMEM/10% FBS with troglitazone. Bar, 200 μm. The graphs below indicate the number of positive colonies/well for ALP and Alizarin red stainings, and of positive cells/cm^2 for oil red O staining. Data are expressed as means (bars) ± SEMs (error bars) for eight wells/group. *, significant difference from the WT culture; $P < 0.01$. **B**: Osteoclastogensis was determined by the number of TRAP-positive multi-nucleated osteoclasts formed in the coculture of bone marrow cells and calvarial osteoblasts from WT and Ad−/− littermates in αMEM/10% FBS with 1,25$(OH)_2D_3$ for 6 days. Bar, 400 μm. Data are expressed as mean (bars) ± SEM (error bars) for eight wells/group. There was no significant difference between WT and Ad−/− cultures. [Color figure can be viewed in the online issue, which is available at www.interscience.wiley.com.]

of IRS-1 and Akt, the main downstream molecules of insulin. Immunoprecipitation and immunoblotting analyses revealed that phosphorylations of IRS-1 and Akt were induced by insulin alone, while hardly being affected by recombinant adiponectin alone. More importantly, the phosphorylations induced by insulin were further enhanced by adiponectin, suggesting indirect/positive action of adiponectin on bone formation via enhancement of the insulin signaling (Fig. 5C).

The results indicate that no bone abnormality in Ad-Tg mice may be possibly due to an equivalent balance of the direct/negative and indirect/positive actions of circulating adiponectin. The direct action might possibly be related to the BMP signaling, and the indirect one may be through enhancement of the insulin signaling.

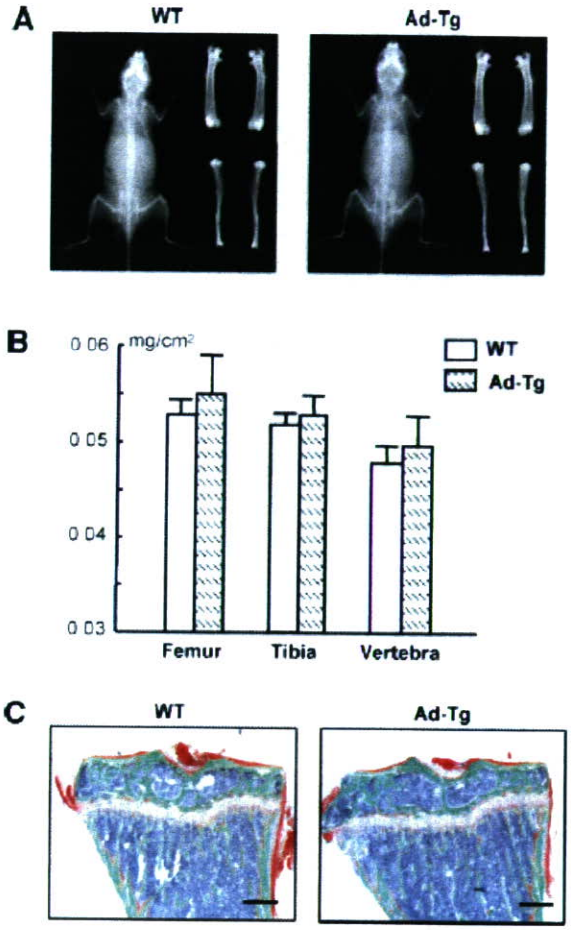

Fig. 4. Radiological and histological findings of the bones in male WT and Ad-Tg littermates (8 weeks old). **A**: Plain X-ray images of the whole bodies (**left**), femurs (**upper right**), and tibiae (**lower right**) of representative WT and Ad-Tg littermates. **B**: BMD of the entire femurs, tibiae, and L2-L5 vertebral bodies determined by DEXA. Data are expressed as means (bars) ± SEM (error bars) of 10 bones/group. None of the bones showed significant difference of BMD between the two genotypes. **C**: Histological features of the proximal tibiae of representative mice of the two genotypes prepared as described in Figure 2. Bar, 100 μm. Data of histomorphometric analyses are shown in Table II. [Color figure can be viewed in the online issue, which is available at www.interscience.wiley.com.]

DISCUSSION

Since we confirmed that adiponectin and its receptors were expressed not only in fat cells but also in bone cells (Fig. 1), the present study examined the actions of adiponectin on bone metabolism separately via autocrine/paracrine and endocrine pathways. To elucidate these distinct actions, we used several in vivo and in vitro systems, and found variable regulations of bone metabolism by adiponectin. First, the Ad−/− mice exhibited no abnormality in the bone, suggesting an equivalent balance of autocrine/paracrine and endocrine actions on bone (Fig. 2). Second, the in vitro adiponectin-deficient marrow cell culture revealed a potent osteogenic effect of adiponectin as an autocrine/paracrine factor (Fig. 3). Third, the lack of bone abnormality in the Ad-Tg mice indicated an equivalent balance of circulating adiponectin (Fig. 4). Lastly, recombinant adiponectin inhibited osteogenesis but enhanced the insulin signaling in osteoprogenitor cell cultures, suggesting the direct/negative and indirect/positive actions of circulating adiponectin on bone formation (Fig. 5). It is therefore speculated that there are at least three distinct adiponectin actions on bone formation: a positive action through the autocrine/paracrine pathway by locally produced adiponectin in bone, a negative action through the direct pathway by circulating adiponectin, and a positive action through the indirect pathway by circulating adiponectin via enhancement of the insulin signaling.

It is of note that effects of adiponectin on bone formation differed among experimental systems, that is, between in vivo and in vitro; between gain-of-function and loss-of-function. These discrepancies are also seen in the actions of leptin, another representative adipokine.

TABLE II. Histomorphometry of Trabecular Bones in Proximal Tibiae of WT and Ad-Tg Mice

	BV/TV (%)	Ob.S/BS (%)	BFR (mm^3/cm^2/year)	Oc.S/BS (%)	ES/BS (%)
WT	11.38 ± 0.67	10.38 ± 0.83	4.96 ± 0.62	5.49 ± 1.39	5.02 ± 0.90
Ad-Tg	13.97 ± 0.62	13.70 ± 1.01	5.06 ± 0.29	6.93 ± 1.87	4.42 ± 1.95

Parameters for the trabecular bone were measured in an area 1.2 mm in length from 250 mm below the growth plate at the proximal metaphysis of the tibiae in Villanueva–Goldner and calcein double-labeled sections. Data expressed as means and standard errors (SEM) for 10 bones/group.
No significant difference of parameters between two genotypes (all $P > 0.05$).
BV/TV, trabecular bone volume expressed as a percentage of total tissue volume; Ob.S/BS, percentage of bone surface covered by cuboidal osteoblasts; BFR, bone formation rate; Oc.S/BS, percentage of bone surface covered by mature osteoclasts; ES/BS, percentage of eroded surface.

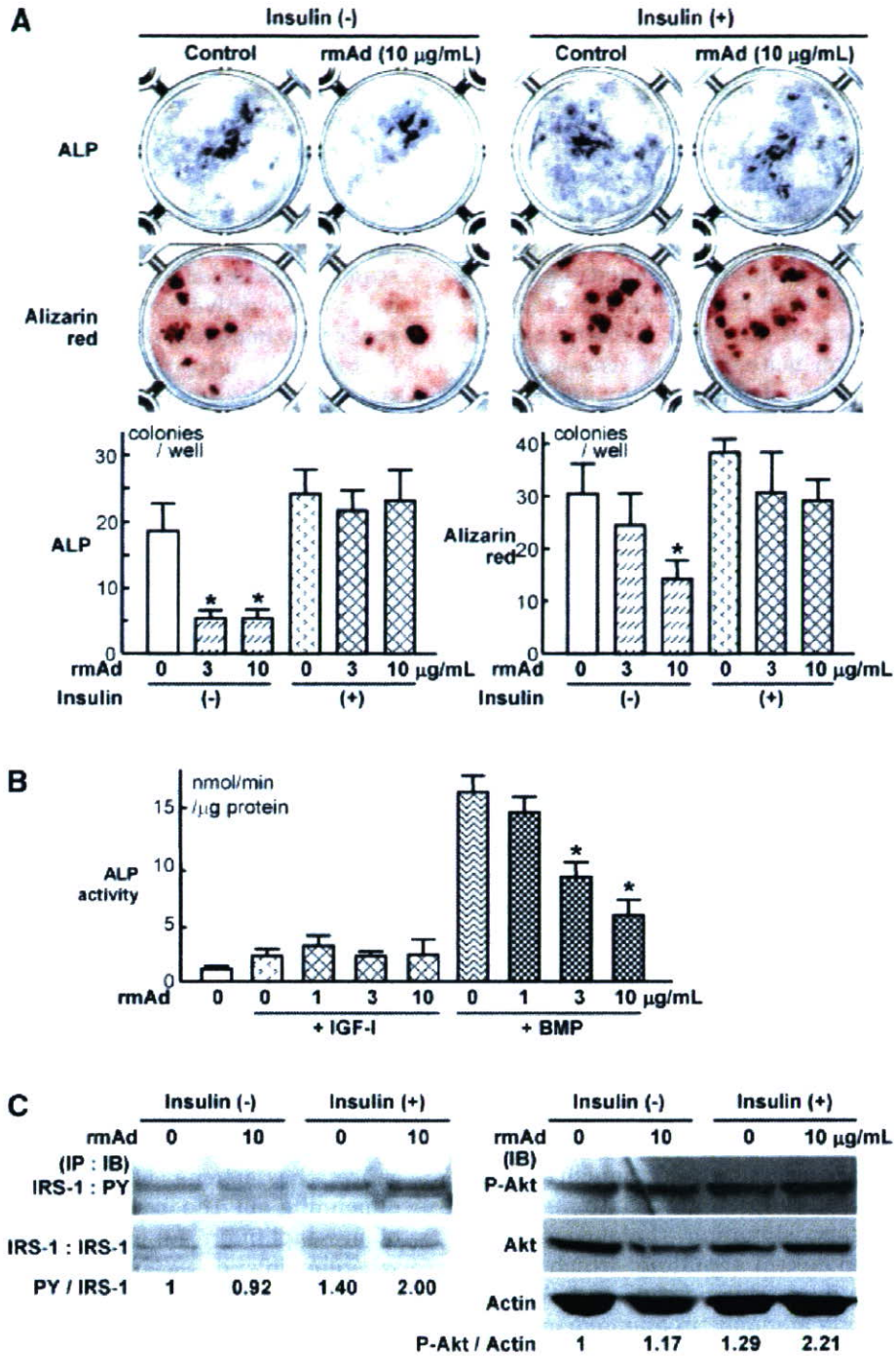

Fig. 5. **A**: Effect of recombinant mouse adiponectin (rmAd) on osteogenesis in the bone marrow cell culture. Osteogenesis was determined by ALP and Alizarin red stainings after 10 and 21 days of culture, respectively, with indicated concentrations of rmAd in αMEM/10% FBS/ascorbic acid/β-glycerophosphate with or without insulin (10 nM). The graphs below indicate the number of positive colonies/well. Data are expressed as means (bars) ± SEMs (error bars) for eight wells/group. *, significant inhibition by rmAd; $P < 0.01$. **B**: Effect of rmAd on ALP activity of ST2 cells cultured for 7 days with indicated concentrations of rmAd in αMEM/10% FBS/ascorbic acid and IGF-1(100 nM) or BMP-2 (10 nM). Data are expressed as means (bars) ± SEMs (error bars) for eight wells/group. *, significant inhibition by rmAd; $P < 0.01$. **C**: Effect of rmAd on phosphorylations of IRS-1 and Akt in cultured bone marrow cells. Protein levels of phosphorylated IRS-1, IRS-1, phosphorylated Akt, Akt, and β-actin were determined by immunoprecipitation (IP) and immunoblotting (IB) in the cells stimulated by insulin (100 nM) or the vehicle for 10 min after pre-treatment with or without rmAd (10 μg/ml) for 24 h. The number under each band shows the ratio of the band intensity of phosphorylated IRS-1 and phosphorylated Akt normalized to those of IRS-1 and β-actin, respectively, that were measured by densitometry. Similar results were obtained in five independent experiments. [Color figure can be viewed in the online issue, which is available at www.interscience.wiley.com.]

Leptin negatively regulates bone formation via a sympathetic nerve system in vivo [Ducy et al., 2000; Takeda et al., 2002; Elefteriou et al., 2004], while recombinant leptin induces osteogenesis in the culture of bone marrow stromal cells [Thomas et al., 1999]. This is implicated to be due to the existence of a circulating soluble leptin receptor that modulates the action of leptin [Kratzsch et al., 2002; Elefteriou et al., 2004]. Although neither soluble receptors nor binding proteins of adiponectin have been identified, it is possible that the co-factors might explain the diverse actions of adiponectin on bone. Another possible mechanism underlying the discrepancy may be a variety of adiponectin forms, since it is present as a full length or as cleavage products such as an active form C-terminal globular fragment in plasma [Fruebis et al., 2001; Kishida et al., 2003]. Although biological activities of the different forms of adiponectin are poorly understood, they might be specific for distinct receptors and cell types. Recently, Oshima et al. [2005] reported that a single injection of adenovirus expressing a full-length adiponectin increased bone mass by stimulating bone formation and suppressing bone resorption. In contrast, the present bone histomorphometric analysis of Ad-Tg mice with constitutive overexpression of the globular form of adiponectin revealed no abnormality in bone formation or bone resorption parameter. This difference may not be due to that of the molecular form since our preliminary investigation of the transgenic mice that overexpress the full-length adiponectin driven by the same SAP promoter also failed to show bone abnormality (unpublished observation by Yamauchi & Kadowaki). We therefore speculate that there may be a compensatory signaling that cancels the excessive adiponectin signaling, which cannot catch up with the acute and strong overexpression by a single adiponectin-adenovirus application.

The present in vitro experiments showed that recombinant full-length adiponectin at the physiological serum concentration (10 μg/ml) [Kubota et al., 2002] inhibited osteogenic differentiation from bone marrow cells and mouse stromal cell line ST2, which is also inconsistent with previous studies showing that it increased the differentiation and mineralization in the murine osteoblast cell line MC3T3-E1 cell and human primary osteoblast cultures [Luo et al., 2005; Oshima et al., 2005]. This might be due to the difference of differentiation stages of cells of osteoblastic lineage. The expression levels of AdipoR1 and AdipoR2 were similar in the precursor cells of the present study, while AdipoR1 was predominantly expressed in the more differentiated osteoblasts of the previous studies. Moreover, although this study implicated the involvement of the BMP pathway, earlier authors reported that the MAP kinase pathway is important for the adiponectin signaling [Luo et al., 2005]. In fact, our study using a mouse calvarial osteoblast culture failed to show the inhibitory effect of the recombinant adiponectin (data not shown). Another explanation for the discrepancy between the present and previous results may be the existence of other lineage of cells than osteoprogenitors in our culture systems, but not in the earlier systems. Because adiponectin is reported to variably regulate differentiation of bone marrow cells into several lineages through the ubiquitously expressed receptors, it is possible that adiponectin can affect other lineage of cells like lymphocytes and adipocytes, causing a proportional decrease of osteoprogenitors in bone marrow. It is known to inhibit B lymphopoiesis through induction of prostaglandin synthesis, but stimulates myelopoiesis [Yokota et al., 2003]. It also suppresses adipogenesis from bone marrow cells through a cyclooxygenase-2/prostaglandin-dependent mechanism [Yokota et al., 2002]; however, the present study showed normal adipogenesis from cultured Ad−/− marrow cells, suggesting the difference of actions of exogenous and endogenous adiponectin on adipogenic differentiation as well. Since the actions of prostaglandins differ depending on the concentration; high doses of prostaglandin suppress collagen synthesis whereas low doses induce it in osteoblasts [Chyun and Raisz, 1984], the actions of adiponectin on bone might be mediated in part by prostaglandin production, so that they differ depending on the concentration. Insofar as the effects of adiponectin on these other types of cells remain unclarified, we should acknowledge that the present study does not reach a definitive conclusion relating to the mechanism of adiponectin on bone homeostasis.

In addition to the direct and negative effect on the osteoprogenitor cells, circulating adiponectin exhibited a positive effect on bone formation through enhancement of the insulin signaling. There is a great deal of evidence supporting that

adiponectin increases the insulin action in its target organs. Recombinant adiponectin ameliorated insulin resistance in obese- and diabetic-KKA^{y} mice and diabetic-lipoatrophic mice, both of which had reduced plasma adiponectin levels [Yamauchi et al., 2001]. A single injection of recombinant adiponectin abolished hyperglycemia by suppressing glucose production in ob/ob, non-obese diabetic, or streptozotocin-treated mice [Berg et al., 2001; Combs et al., 2001]. Transgenic overexpression of adiponectin also ameliorated insulin resistance in ob/ob mice [Yamauchi et al., 2003b] and the disruption of the adiponectin gene is known to cause insulin resistance [Matsuzawa et al., 2004; Luo et al., 2005]. Another plausible hormone that might be related to the endocrine action of adiponectin might be estrogen, which is also a potent regulator of bone metabolism [Tanko and Christiansen, 2004]. A recent report demonstrated that estrogen can suppress adiponectin secretion in mice and cultured adipocytes [Combs et al., 2003], although the interactions of signalings among adiponectin, estradiol, and insulin in bone are complicated and remain to be further clarified [Kalish et al., 2003].

Regarding the clinical evidence of involvement of adiponectin in bone metabolism, Kontogianni et al. [2004] reported that the circulating level of adiponectin was not correlated with bone mass of perimenopausal women while that of leptin showed an inverse correlation. This is in accordance with the present results that both deficient and overexpressing transgenic mice of adiponectin showed normal bone mass. However, another clinical study by Lenchik et al. [2003] reported significant inverse correlations of adiponectin with visceral fat and BMD, and proposed adiponectin as a mediator of the protective effects of visceral fat mass on BMD. The correlations may be dependent on the balance of the direct and indirect actions of circulating adiponectin, which we showed oppositely affected bone metabolism. When we compare the populations of the two clinical studies above, more subjects (86%) in the study by Lenchik et al. were affected by type 2 diabetes than those in the study by Kontogianni et al. This might at least partly explain the discrepancy of the two clinical studies: in the former the indirect and positive effect of circulating adiponectin was suppressed due to the impaired insulin signaling, so that the direct and negative effect became predominant, while in the latter study there remained an equivalent balance between direct and indirect effects.

Adiponectin is structurally similar to TNF-α, receptor activator of nuclear factor κB ligand (RANKL) and osteoprotegerin, all of which are potent regulators of osteoclastogenesis [Ouchi et al., 2000; Tsao et al., 2002]. However, osteoclastogenesis from marrow cells was not affected by the deficiency of endogenous adiponectin (Ad−/−) in the present study, while a previous study showed a decrease of osteoclastogenesis by adiponectin in vivo and in vitro [Oshima et al., 2005]. This also indicates that there might be distinct effects of adiponectin on osteoclastogenesis through autocrine/paracrine and endocrine pathways. Considering that adiponectin expression is regulated by several bone regulators: it is reduced by TNF-α [Yokota et al., 2000], IL-6 [Kappes and Loffler, 2000], β-adrenergic agonists [Fasshauer et al., 2003], and glucocorticoids [Halleux et al., 2001], whereas stimulated by proliferator-activated receptor (PPARγ) agonists [Combs et al., 2002], adiponectin may play a role in the complicated molecular network that regulates bone metabolism.

ACKNOWLEDGMENTS

We thank Reiko Yamaguchi for providing expert technical assistance. Regrettably, Masayuki Yamaguchi died much young and before the publication of this study. We dedicate this study to him and his family. This work was supported by Grant-in-Aid for Scientific Research from the Japanese Ministry of Education, Culture, Sports, Science, and Technology Grant no. 17591551.

REFERENCES

Arita Y, Kihara S, Ouchi N, Takahashi M, Maeda K, Miyagawa J, Hotta K, Shimomura I, Nakamura T, Miyaoka K, Kuriyama H, Nishida M, Yamashita S, Okubo K, Matsubara K, Muraguchi M, Ohmoto Y, Funahashi T, Matsuzawa Y. 1999. Paradoxical decrease of an adipose-specific protein, adiponectin, in obesity. Biochem Biophys Res Commun 257:79–83.

Berg AH, Combs TP, Du X, Brownlee M, Scherer PE. 2001. The adipocyte-secreted protein Acrp30 enhances hepatic insulin action. Nat Med 7:947–953.

Berner HS, Lyngstadaas SP, Spahr A, Monjo M, Thommesen L, Drevon CA, Syversen U, Reseland JE. 2004. Adiponectin and its receptors are expressed in bone-forming cells. Bone 35:842–849.

Chyun YS, Raisz LG. 1984. Stimulation of bone formation by prostaglandin E2. Prostaglandins 27:97–103.

Combs TP, Berg AH, Obici S, Scherer PE, Rossetti L. 2001. Endogenous glucose production is inhibited by the adipose-derived protein Acrp30. J Clin Invest 108: 1875–1881.

Combs TP, Wagner JA, Berger J, Doebber T, Wang WJ, Zhang BB, Tanen M, Berg AH, O'Rahilly S, Savage DB, Chatterjee K, Weiss S, Larson PJ, Gottesdiener KM, Gertz BJ, Charron MJ, Scherer PE, Moller DE. 2002. Induction of adipocyte complement-related protein of 30 kilodaltons by PPARgamma agonists: A potential mechanism of insulin sensitization. Endocrinology 143: 998–1007.

Combs TP, Berg AH, Rajala MW, Klebanov S, Iyengar P, Jimenez-Chillaron JC, Patti ME, Klein SL, Weinstein RS, Scherer PE. 2003. Sexual differentiation, pregnancy, calorie restriction, and aging affect the adipocyte-specific secretory protein adiponectin. Diabetes 52:268–276.

Diez JJ, Iglesias P. 2003. The role of the novel adipocyte-derived hormone adiponectin in human disease. Eur J Endocrinol 148:293–300.

Ducy P, Amling M, Takeda S, Priemel M, Schilling AF, Beil FT, Shen J, Vinson C, Rueger JM, Karsenty G. 2000. Leptin inhibits bone formation through a hypothalamic relay: A central control of bone mass. Cell 100:197–207.

Elefteriou F, Takeda S, Ebihara K, Magre J, Patano N, Kim CA, Ogawa Y, Liu X, Ware SM, Craigen WJ, Robert JJ, Vinson C, Nakao K, Capeau J, Karsenty G. 2004. Serum leptin level is a regulator of bone mass. Proc Natl Acad Sci USA 101:3258–3263.

Fasshauer M, Kralisch S, Klier M, Lossner U, Bluher M, Klein J, Paschke R. 2003. Adiponectin gene expression and secretion is inhibited by interleukin-6 in 3T3-L1 adipocytes. Biochem Biophys Res Commun 301:1045–1050.

Felson DT, Zhang Y, Hannan MT, Anderson JJ. 1993. Effects of weight and body mass index on bone mineral density in men and women: The Framingham study. J Bone Miner Res 8:567–573.

Fruebis J, Tsao TS, Javorschi S, Ebbets-Reed D, Erickson MR, Yen FT, Bihain BE, Lodish HF. 2001. Proteolytic cleavage product of 30-kDa adipocyte complement-related protein increases fatty acid oxidation in muscle and causes weight loss in mice. Proc Natl Acad Sci USA 98:2005–2010.

Halleux CM, Takahashi M, Delporte ML, Detry R, Funahashi T, Matsuzawa Y, Brichard SM. 2001. Secretion of adiponectin and regulation of apM1 gene expression in human visceral adipose tissue. Biochem Biophys Res Commun 288:1102–1107.

Hotta K, Funahashi T, Arita Y, Takahashi M, Matsuda M, Okamoto Y, Iwahashi H, Kuriyama H, Ouchi N, Maeda K, Nishida M, Kihara S, Sakai N, Nakajima T, Hasegawa K, Muraguchi M, Ohmoto Y, Nakamura T, Yamashita S, Hanafusa T, Matsuzawa Y. 2000. Plasma concentrations of a novel, adipose-specific protein, adiponectin, in type 2 diabetic patients. Arterioscler Thromb Vasc Biol 20: 1595–1599.

Hu E, Liang P, Spiegelman BM. 1996. AdipoQ is a novel adipose-specific gene dysregulated in obesity. J Biol Chem 271:10697–10703.

Kalish GM, Barrett-Connor E, Laughlin GA, Gulanski BI. 2003. Association of endogenous sex hormones and insulin resistance among postmenopausal women: Results from the postmenopausal estrogen/progestin intervention trial. J Clin Endocrinol Metab 88:1646–1652.

Kappes A, Loffler G. 2000. Influences of ionomycin, dibutyryl-cycloAMP and tumour necrosis factor-alpha on intracellular amount and secretion of apM1 in differentiating primary human preadipocytes. Horm Metab Res 32:548–554.

Kharroubi I, Rasschaert J, Eizirik DL, Cnop M. 2003. Expression of adiponectin receptors in pancreatic beta cells. Biochem Biophys Res Commun 312:1118–1122.

Kishida K, Nagaretani H, Kondo H, Kobayashi H, Tanaka S, Maeda N, Nagasawa A, Hibuse T, Ohashi K, Kumada M, Nishizawa H, Okamoto Y, Ouchi N, Maeda K, Kihara S, Funahashi T, Matsuzawa Y. 2003. Disturbed secretion of mutant adiponectin associated with the metabolic syndrome. Biochem Biophys Res Commun 306:286–292.

Kobayashi K, Takahashi N, Jimi E, Udagawa N, Takami M, Kotake S, Nakagawa N, Kinosaki M, Yamaguchi K, Shima N, Yasuda H, Morinaga T, Higashio K, Martin TJ, Suda T. 2000. Tumor necrosis factor alpha stimulates osteoclast differentiation by a mechanism independent of the ODF/RANKL-RANK interaction. J Exp Med 191: 275–286.

Kontogianni MD, Dafni UG, Routsias JG, Skopouli FN. 2004. Blood leptin and adiponectin as possible mediators of the relation between fat mass and BMD in perimenopausal women. J Bone Miner Res 19:546–551.

Kratzsch J, Lammert A, Bottner A, Seidel B, Mueller G, Thiery J, Hebebrand J, Kiess W. 2002. Circulating soluble leptin receptor and free leptin index during childhood, puberty, and adolescence. J Clin Endocrinol Metab 87:4587–4594.

Kubota N, Terauchi Y, Yamauchi T, Kubota T, Moroi M, Matsui J, Eto K, Yamashita T, Kamon J, Satoh H, Yano W, Froguel P, Nagai R, Kimura S, Kadowaki T, Noda T. 2002. Disruption of adiponectin causes insulin resistance and neointimal formation. J Biol Chem 277:25863–25866.

Lenchik L, Register TC, Hsu FC, Lohman K, Nicklas BJ, Freedman BI, Langefeld CD, Carr JJ, Bowden DW. 2003. Adiponectin as a novel determinant of bone mineral density and visceral fat. Bone 33:646–651.

Luo XH, Guo LJ, Yuan LQ, Xie H, Zhou HD, Wu XP, Liao EY. 2005. Adiponectin stimulates human osteoblasts proliferation and differentiation via the MAPK signaling pathway. Exp Cell Res 309:99–109.

Maeda K, Okubo K, Shimomura I, Funahashi T, Matsuzawa Y, Matsubara K. 1996. cDNA cloning and expression of a novel adipose specific collagen-like factor, apM1 (AdiPose Most abundant Gene transcript 1). Biochem Biophys Res Commun 221:286–289.

Matsubara M, Maruoka S, Katayose S. 2002. Inverse relationship between plasma adiponectin and leptin concentrations in normal-weight and obese women. Eur J Endocrinol 147:173–180.

Matsuzawa Y, Funahashi T, Kihara S, Shimomura I. 2004. Adiponectin and metabolic syndrome. Arterioscler Thromb Vasc Biol 24:29–33.

Nakano Y, Tobe T, Choi-Miura NH, Mazda T, Tomita M. 1996. Isolation and characterization of GBP28, a novel gelatin-binding protein purified from human plasma. J Biochem (Tokyo) 120:803–812.

Oshima K, Nampei A, Matsuda M, Iwaki M, Fukuhara A, Hashimoto J, Yoshikawa H, Shimomura I. 2005. Adiponectin increases bone mass by suppressing osteoclast and activating osteoblast. Biochem Biophys Res Commun 331:520–526.

Ouchi N, Kihara S, Arita Y, Okamoto Y, Maeda K, Kuriyama H, Hotta K, Nishida M, Takahashi M, Muraguchi M, Ohmoto Y, Nakamura T, Yamashita S, Funahashi T, Matsuzawa Y. 2000. Adiponectin, an adipocyte-derived plasma protein, inhibits endothelial NF-kappaB signaling through a cAMP-dependent pathway. Circulation 102:1296–1301.

Parfitt AM, Drezner MK, Glorieux FH, Kanis JA, Malluche H, Meunier PJ, Ott SM, Recker RR. 1987. Bone histomorphometry: Standardization of nomenclature, symbols, and units. Report of the ASBMR Histomorphometry Nomenclature Committee. J Bone Miner Res 2: 595–610.

Scherer PE, Williams S, Fogliano M, Baldini G, Lodish HF. 1995. A novel serum protein similar to C1q, produced exclusively in adipocytes. J Biol Chem 270:26746–26749.

Takeda S, Elefteriou F, Levasseur R, Liu X, Zhao L, Parker KL, Armstrong D, Ducy P, Karsenty G. 2002. Leptin regulates bone formation via the sympathetic nervous system. Cell 111:305–317.

Tanko LB, Christiansen C. 2004. Can confounding with fat-derived endogenous free estradiol explain the inverse correlation of bone mineral density with adiponectin? Bone 34:916; author reply 917.

Thomas DM, Hards DK, Rogers SD, Ng KW, Best JD. 1996. Insulin receptor expression in bone. J Bone Miner Res 11:1312–1320.

Thomas T, Gori F, Khosla S, Jensen MD, Burguera B, Riggs BL. 1999. Leptin acts on human marrow stromal cells to enhance differentiation to osteoblasts and to inhibit differentiation to adipocytes. Endocrinology 140:1630–1638.

Tremollieres FA, Pouilles JM, Ribot C. 1993. Vertebral postmenopausal bone loss is reduced in overweight women: A longitudinal study in 155 early postmenopausal women. J Clin Endocrinol Metab 77:683–686.

Tsao TS, Murrey HE, Hug C, Lee DH, Lodish HF. 2002. Oligomerization state-dependent activation of NF-kappa B signaling pathway by adipocyte complement-related protein of 30 kDa (Acrp30). J Biol Chem 277:29359–29362.

Ukkola O, Santaniemi M. 2002. Adiponectin: A link between excess adiposity and associated comorbidities? J Mol Med 80:696–702.

Weyer C, Funahashi T, Tanaka S, Hotta K, Matsuzawa Y, Pratley RE, Tataranni PA. 2001. Hypoadiponectinemia in obesity and type 2 diabetes: Close association with insulin resistance and hyperinsulinemia. J Clin Endocrinol Metab 86:1930–1935.

Yamauchi T, Kamon J, Waki H, Terauchi Y, Kubota N, Hara K, Mori Y, Ide T, Murakami K, Tsuboyama-Kasaoka N, Ezaki O, Akanuma Y, Gavrilova O, Vinson C, Reitman ML, Kagechika H, Shudo K, Yoda M, Nakano Y, Tobe K, Nagai R, Kimura S, Tomita M, Froguel P, Kadowaki T. 2001. The fat-derived hormone adiponectin reverses insulin resistance associated with both lipoatrophy and obesity. Nat Med 7:941–946.

Yamauchi T, Kamon J, Ito Y, Tsuchida A, Yokomizo T, Kita S, Sugiyama T, Miyagishi M, Hara K, Tsunoda M, Murakami K, Ohteki T, Uchida S, Takekawa S, Waki H, Tsuno NH, Shibata Y, Terauchi Y, Froguel P, Tobe K, Koyasu S, Taira K, Kitamura T, Shimizu T, Nagai R, Kadowaki T. 2003a. Cloning of adiponectin receptors that mediate antidiabetic metabolic effects. Nature 423:762–769.

Yamauchi T, Kamon J, Waki H, Imai Y, Shimozawa N, Hioki K, Uchida S, Ito Y, Takakuwa K, Matsui J, Takata M, Eto K, Terauchi Y, Komeda K, Tsunoda M, Murakami K, Ohnishi Y, Naitoh T, Yamamura K, Ueyama Y, Froguel P, Kimura S, Nagai R, Kadowaki T. 2003b. Globular adiponectin protected ob/ob mice from diabetes and ApoE-deficient mice from atherosclerosis. J Biol Chem 278:2461–2468.

Yokota T, Oritani K, Takahashi I, Ishikawa J, Matsuyama A, Ouchi N, Kihara S, Funahashi T, Tenner AJ, Tomiyama Y, Matsuzawa Y. 2000. Adiponectin, a new member of the family of soluble defense collagens, negatively regulates the growth of myelomonocytic progenitors and the functions of macrophages. Blood 96:1723–1732.

Yokota T, Meka CS, Medina KL, Igarashi H, Comp PC, Takahashi M, Nishida M, Oritani K, Miyagawa J, Funahashi T, Tomiyama Y, Matsuzawa Y, Kincade PW. 2002. Paracrine regulation of fat cell formation in bone marrow cultures via adiponectin and prostaglandins. J Clin Invest 109:1303–1310.

Yokota T, Meka CS, Kouro T, Medina KL, Igarashi H, Takahashi M, Oritani K, Funahashi T, Tomiyama Y, Matsuzawa Y, Kincade PW. 2003. Adiponectin, a fat cell product, influences the earliest lymphocyte precursors in bone marrow cultures by activation of the cyclooxygenase-prostaglandin pathway in stromal cells. J Immunol 171:5091–5099.

GENE DELIVERY

ELSEVIER

Available online at www.sciencedirect.com
SCIENCE DIRECT®

Journal of Controlled Release 111 (2006) 368–370

journal of controlled release

www.elsevier.com/locate/jconrel

Rapid communication

Organic–inorganic hybrid-nanocarrier of siRNA constructing through the self-assembly of calcium phosphate and PEG-based block aniomer

Yoshinori Kakizawa [a], Sanae Furukawa [a], Atushi Ishii [b,c], Kazunori Kataoka [c,d,e,*]

[a] *Biomaterials Center, National Institute for Materials Science, 1-1 Namiki, Tsukuba, Ibaraki 305-0044, Japan*
[b] *NanoCarrier Co., 5-4-19 Kashiwanoha, Kashiwa, Chiba 277-0882, Japan*
[c] *Department of Materials Engineering, Graduate School of Engineering, The University of Tokyo, 7-3-1 Hongo, Bunkyo-ku, Tokyo 113-8656, Japan*
[d] *Division of Clinical Biotechnology, Center for Disease Biology and Integrative Medicine, Graduate School of Medicine, The University of Tokyo, 7-3-1 Hongo, Bunkyo-ku, Tokyo 113-0033, Japan*
[e] *Center for NanoBio Integration, The University of Tokyo, 7-3-1 Hongo, Bunkyo-ku, Tokyo, 113-8656, Japan*

Received 30 October 2005; accepted 16 January 2006
Available online 28 February 2006

Abstract

The development of siRNA delivery systems is a major key for practical RNA therapy that holds promise for the treatment of life-threatening human diseases, yet there still exists significant difficulties in their construction because of the various requirements including high transfection efficacy, tolerability in the biological medium, and low toxicity. Here we report the novel preparation route of organic–inorganic hybrid-nanocarriers entrapping siRNA based on the self-assembly of the block aniomer, poly(ethylene glycol)-*block*-poly(methacrylic acid), with calcium phosphate crystals. The nanocarriers have diameters in the range of several hundreds of nanometers and revealed excellent colloidal stability due to the steric stabilization effect of the PEG palisade. The biological activity of siRNA loaded in nanocarriers was assessed using 293 cells stably expressing luciferase gene, showing the remarkably high gene silencing-efficacy without the use of any adjuvant molecules such as chroloquin. Further advantage of the system is the serum tolerability, which is of a critical issue in in vivo application.

Short interfering RNA (siRNA) that mediates gene-silencing phenomena of RNA interference (RNAi) needs a carrier system to exert biological activity, especially, for in vivo application [1]. Some lipid- and polymer-based systems are available for the in vitro application of siRNA, yet they often have drawbacks including a low stability in a serum-containing medium and significant cytotoxicity. From the standpoint of developing a safe and serum-tolerable carrier system, the calcium phosphate (CaP) co-precipitation method is of interest [2]. To control the growth of CaP, that is the determining factor for the transfection efficacy, a novel concept has recently been introduced by our group based on the self-assembly of poly(ethylene glycol)-*block*-poly(aspartic acid) block copolymers (PEG-P(Asp)) with CaP to form the narrowly distributed hybrid nanoparticles covered with PEG palisades [3].

siRNA-entrapped PEG-P(Asp)/CaP hybrid nanoparticles indeed revealed an appreciable gene silencing in a cultured cell line [4]. Nevertheless, the requirement of chroloquin, a reagent facilitating endosomal-escape, impedes the wide applicability of this method. Herein, we overcome this critical issue using the newly designed system of siRNA-entrapped CaP nanoparticles. The strategy is to incorporate the molecular units facilitating endosomal-escape directly into the block copolymer structure. In this regard, poly(methacrylic acid) (PMA) was selected as the polyanion unit in the block copolymer. PMA undergoes a conformational transition at pH 4–6, which almost corresponds to the endosomal pH, to adopt a more hydrophobic conformation as compared to neutral pH, thus expected to have an increased interaction with the endosomal membrane in order to perturb its structure to facilitate escape of the nanoparticles into the cytoplasm [5]. Here, two different compositions of the poly(ethylene glycol)-*block*-poly(methacrylic acid) (PEG-PMA) were used for the nanoparticle formation entrapping siRNA. PEG-PMA1 has a PEG segment with the molecular weight (Mw) of 7800 and the PMA segment with the Mw of

* Corresponding author. Department of Materials Engineering, Graduate School of Engineering, The University of Tokyo, 7-3-1 Hongo, Bunkyo-ku, Tokyo 113-8656, Japan.
E-mail address: kataoka@bmw.t.u-tokyo.ac.jp (K. Kataoka).

0168-3659/$ - see front matter © 2006 Elsevier B.V. All rights reserved.
doi:10.1016/j.jconrel.2006.01.004

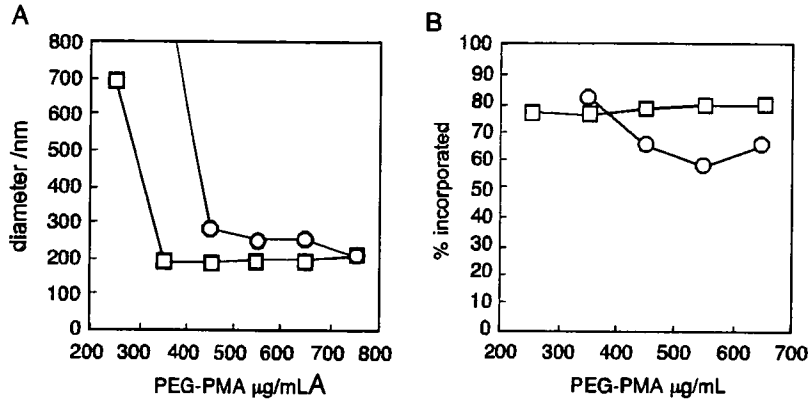

Fig. 1. Physicochemical characterization of nanoparticles composed of PEG-PMA1 (□) and PEG-PMA2 (○). (A) Size of the nanoparticles entrapping siRNA determined by DLS measurements. (B) Percentage of siRNA loaded in the nanoparticles formed at varying PEG-PMA concentrations.

2000, while the Mw of the PEG and PMA segments of PEG-PMA2 are 7500 and 15,500, respectively.

The diameters of the nanoparticles formed in the presence of the PEG-PMAs are determined by dynamic light scattering measurements [6,7]. Fig. 1A shows the change in diameters of nanoparticles with varying concentrations of PEG-PMAs at 3.0 mM phosphate. A similar trend was observed for PEG-PMA1 and PEG-PMA2, and the stable dispersion of nanoparticles was obtained over certain concentrations; 350 μg/mL for PEG-PMA1 and 450 μg/mL for PEG-PMA2. Diameters above these critical concentrations of PEG-PMA were about 180–200 and 200–280 nm for PEG-PMA1 and PEG-PMA2, respectively. It is noteworthy that at those concentrations no precipitation of CaP was observed 24 h after the mixing of Ca/siRNA and phosphate/PEG-PMA solution. The polydispersity indices of the nanoparticles were below 0.1 for PEG-PMA1, suggesting a unimodal distribution, while the values were slightly higher (0.12–0.15) for PEG-PMA2. The zeta potential of nanoparticles composed of 450 μg/mL of PEG-PMA1 or PEG-PMA2 was almost zero, −1.50±0.36 and −0.439±0.118 mV, respectively, indicating that the colloidal stability of the nanoparticles is caused by the PEG palisades with the steric repulsion effect. The incorporation efficacy of siRNA in the nanoparticles determined by the centrifugation method was around 80% for PEG-PMA1 and 60–80% for PEG-PMA2 [8] (Fig. 1B).

In order to investigate RNAi activity of siRNA incorporated in the nanoparticles, we have established a 293 cell line stably expressing the GL3-luciferase gene and estimated the degree of gene silencing using the siRNA targeting GL3-luciferase gene [9–11] . Fig. 2A shows the effect of the PEG-PMA concentrations on the RNAi activity of the siRNA-loaded nanoparticles, expressed as the relative inhibition activity to the control (non-silencing) siRNA. PEG-PMA1 showed no remarkable RNAi activity (■), while the PEG-PMA2 system (●) achieved a gene silencing down to 20% of the control (80% inhibition) in the polymer concentration range of 450 to 550 μg/mL. The

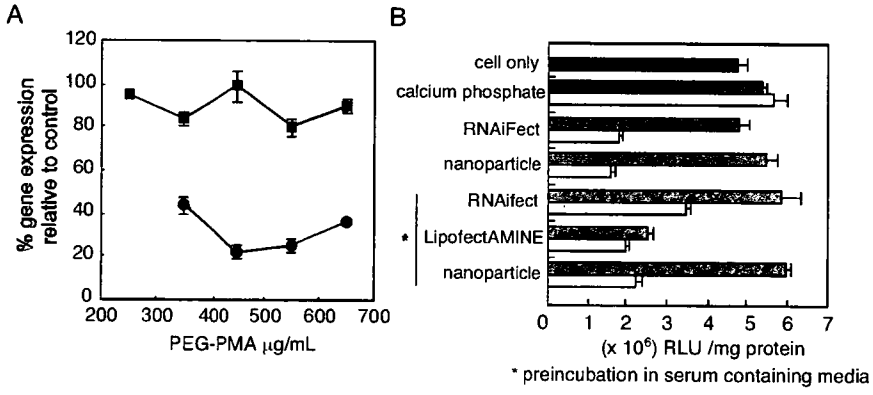

Fig. 2. Biological activity of siRNA incorporated in nanoparticles. (A) RNA interference by siRNA incorporated in nanoparticles formed at various concentrations of PEG-PMAs. GL3 luciferase gene expression in 293 cells was inhibited by nanoparticles composed of PEG-PMA1 (■) and PEG-PMA2 (●). Results are shown as the percentage to the control expression of cells treated with nanoparticles entrapping non-silencing siRNA. (B) RNA interference by siRNA using various transfection reagents. Grey bars indicate GL3 luciferase gene expressions in 293 cells treated with non-silencing control siRNA, and white bars indicate those treated with GL3 siRNA. The nanoparticle samples are composed of calcium phosphate and PEG-PMA2 formed at 450 μg/mL. For the preincubation study (*), DMEM containing 20% FCS was added to an equal amount of nanoparticle or lipoplex solutions and incubated at 37 °C for 30 min prior to the transfection. In the calcium phosphate method, the transfection was performed under the same condition as the nanoparticle except in the absence of PEG-PMA. The concentrations of siRNA and calcium ion in all the experiments were 125 nM and 6.25 mM, respectively.

reason for the presence of the maximum transfection efficacy in terms of the PEG-PMA concentration is not yet clear, however, nanoparticles with smaller diameters seem to be more efficient than the larger CaP/PEG-PMA complex or precipitate formed at the lower PEG-PMA concentration. For example, at 250 μg/mL PEG-PMA1, at which a large precipitate was formed, no silencing was recognized. The siRNA concentration dependency was evaluated using the sample solutions prepared by dilution of the stock nanoparticle solution formed at 450 μg/mL of PEG-PMA2 and 2.5 μM of siRNA. The significant inhibition was observed at a concentration as low as 6.7 nM (45% inhibition) and reached a plateau value around 25 nM (80% inhibition).

To clarify the advantages of this system, the transfection efficacy was further compared with other transfection reagents and the conventional calcium phosphate method (Fig. 2B). Under the experimental conditions, the hybrid nanoparticles formed at 450 μg/mL of PEG-PMA showed transfection efficacy similar to RNAiFect. Worth noting is that the nanoparticles are more efficient in silencing than RNAiFect at the more physiologically relevant conditions: Preincubation in the DMEM containing 10% FCS was performed for 30 min prior to the transfection (*—marked conditions in Fig. 2B). Upon serum pre-incubation, the GL3 luciferase expression relative to the control increased from 36% to 58% in the case of RNAiFect, while the increase is only 29% to 35% for the hybrid nanoparticle system. Another type of lipid-based transfection reagent, lipofectAMINE, showed a non-specific effect in the serum-containing medium, which resulted in a significantly reduced luciferase activity even using the controlled non-silencing siRNA, presumably due to the toxicity. Tolerability to the serum is crucial when considering the in vivo application of the carrier system, especially, in the case of the systemic administration. Indeed, the in vivo application of a conventionally available cationic-lipid system is reported to be hampered in the serum-containing medium [12]. Furthermore, no significant activity of siRNA was observed for the calcium phosphate crystal prepared in the absence of PEG-PMA, indicating the necessity of the block copolymer for the improved transfection activity.

In summary, we demonstrated a highly efficient transfection of siRNA to cultured mammalian cells using nano-sized calcium phosphate crystals with appreciable serum tolerability. This nano-particulate siRNA carrier possessing a biocompatible PEG palisade and a pH-responsive moiety of PMA to facilitate endosomal escape may have a promising utility in RNAi research directed toward disease treatment.

Acknowledgements

This work was supported in part by the Core Research for Evolution of Science and Technology (CREST), Japan Science and Technology Corporation (JST) and by the Project on Material Development for Innovative Nano-Drug Delivery Systems, The Ministry of Education, Culture, Sports, Science and Technology, Japan (MEXT).

References

[1] F. Simeoni, M.C. Morris, F. Heitz, G. Divita, Nucleic Acids Res. 31 (2003) 2717–2724;
D.R. Sørensen, M. Leirdal, M. Sioud, J. Mol. Biol. 327 (2003) 761–766.
[2] C. Chen, H. Okayama, Mol. Cell. Biol. 7 (1987) 2745–2752;
H. Tolou, Anal. Biochem. 215 (1993) 156–158.
[3] Y. Kakizawa, K. Kataoka, Langmuir 18 (2002) 4539–4543.
[4] Y. Kakizawa, S. Furukawa, K. Kataoka, J. Control. Release 97 (2004) 345–356.
[5] M. Mandel, J.C. Leyte, M.G. Standhouder, J. Phys. Chem. 71 (1967) 603–612;
A.F. Olea, H. Rosenbluth, J.K. Thomas, Macromolecules 32 (1999) 8077–8083.
[6] The nanoparticles were prepared as follows: A solution of 2.5 M $CaCl_2$ was added to a solution of siRNA in a buffer (1 mM Tris–HCl, 0.1 mM EDTA, pH 7.6) to a final volume (Ca^{2+} 250 mM, siRNA 74 μg/mL). One volume of this 2× Ca/siRNA solution was quickly added to an equal volume of 2× Hepes/phosphate/PEG-PMA solution (140 mM NaCl, 50 mM HEPES, 6.0 mM Na_2HPO_4, PEG-PMA, pH 7.1). The mixed solutions were vigorously stirred by a vortex mixer for a few seconds and incubated at 37 °C for 24 h.
[7] D.E. Koppel, J. Chem. Phys. 57 (1972) 4814–4820.
[8] siRNA content was determined as follows: The sample solutions (200 μL) were centrifuged at 15000 ×*g* for 30 min to precipitate the nanoparticles. Supernatants (100 μL) were carefully removed to determine siRNA concentration by absorbance at 260 nm. The percentage of the loaded siRNA was calculated by subtracting the siRNA concentration in the supernatant from the total concentration.
[9] siRNA targeting GL3-luciferase gene, antisense sequence; 5′-UCGAA GUACUCAGCGUAAGdTdT-3′, sense sequence; 5′-CUUACGCUGA GUACUUCGAdTdT-3′, control (non-silencing) siRNA; antisense sequence; 5′-UUCUCCGAACGUGUCACGUdTdT-3′, sense sequence; 5′-ACGUGACACGUUCGGAGAAdTdT-3′).
[10] S.M. Elbashir, J. Harboth, W. Lendeckel, A. Yalcin, K. Weber, T. Tuschl, Nature 11 (2001) 494–498.
[11] The 293 cell line stably expressing GL3-luciferase gene was established using Flp-In system (Invitrogen) according to the manufacturer's protocol. The cells were plated at the density of ~8×10^3 cells/well in a 96 well plate and grown overnight in medium containing 10% FCS. Before transfection, the medium was removed and 50 μL of fresh medium containing 20% FCS was added to each well. The stock nanoparticle solutions (siRNA 2.5 μM) were diluted with DMEM to desired concentrations. Fifty microliters of the diluted sample solutions were added to each well and the cells were incubated at 37 °C for 42 h under 5% CO_2 atmosphere. Luciferase gene expression was measured using Luciferase assay kit from Promega. Protein concentration was determined by BCA protein assay kit from Pierce. For the commercially available transfection reagents, RNAiFect and LipofectAMINE, transfection experiments were performed following a protocol provided by the manufacturer. The conventional calcium phosphate coprecipitation method was performed as Jordan et al. reported (Jordan, M.; Schallhorn, A.; Wurm, F. M. Nucleic Acids Res. 1996, 24, 596–601).
[12] A. Chonn, S.C. Semple, P.R. Cullis, J. Biol. Chem. 267 (1992) 18759–18765;
S. Li, W.C. Tseng, D.B. Stolz, S.P. Wu, S.C. Watkins, L. Huang, Gene Ther. 6 (1999) 585–594.

Intraarticular Injection of High Molecular Weight Hyaluronan for Osteoarthritis of the Knee — Prediction of Effectiveness with Biological Markers

HARUO SUGIMOTO, HARUMOTO YAMADA, NOBUKI TERADA, ARIHIKO KANAJI, SHINICHI KATO, HIDEKI DATE, HIROFUSA ICHINOSE, and KYOSUKE MIYAZAKI

Reprinted from THE JOURNAL OF RHEUMATOLOGY

Volume 33, Number 12, December 2006

Pages 2527–2531

Intraarticular Injection of High Molecular Weight Hyaluronan for Osteoarthritis of the Knee — Prediction of Effectiveness with Biological Markers

HARUO SUGIMOTO, HARUMOTO YAMADA, NOBUKI TERADA, ARIHIKO KANAJI, SHINICHI KATO, HIDEKI DATE, HIROFUSA ICHINOSE, and KYOSUKE MIYAZAKI

ABSTRACT. ***Objective.*** The possibility of predicting the effectiveness of intraarticular injection of high molecular weight hyaluronan (HA) was investigated using biological markers.

Methods. In 32 patients with osteoarthritis (OA) of the knee, 38 knees were treated with HA injection, and the clinical symptoms were evaluated using the Japanese Orthopaedic Association (JOA) score and pain visual analog scale (VAS). The concentrations of chondroitin 6-sulfate, 4-sulfate (C6S, C4S), and aggrecan were measured in synovial fluid collected at the time of initiation of injection. The relationship between the biological markers and the improvement of clinical symptoms after injection for 1 month was investigated.

Results. C6S/C4S and concentration of aggrecan decreased after injection, although these decreases were not significant. Positive correlations were noted between the concentrations of C6S and aggrecan before HA injection and the improvement of the JOA score after injection; however, radiological OA stage had no significant relation with improvement both of the JOA score and VAS.

Conclusion. It has been reported that the concentration of aggrecan-derived fragments in synovial fluid decreases with advancement of the OA stage, reflecting decreases in the amount of residual cartilage and suppression of chondrocyte metabolism. Our findings suggested that HA injection exhibits a greater clinical effect in cases with a high intraarticular aggrecan fragment concentration, i.e., cases in which a high amount of residual cartilage and chondrocyte metabolic activity remain.The biological markers were useful in predicting the effectiveness of HA injection for OA of the knee. (J Rheumatol 2006;33:2527–31)

Key Indexing Terms:
OSTEOARTHRITIS HYALURONAN SYNOVIAL FLUID
MARKER PREDICTION INTRAARTICULAR INJECTION THERAPY

The prevalence of osteoarthritis (OA) has increased markedly with the rapid shift towards the elderly in industrially advanced countries. The major lesion of OA involves degeneration and destruction of cartilage. The early process of destruction of cartilage in OA involves degradation and conversion to lower molecular weight cartilage matrix, such as type II collagen and aggrecan, that maintains the mechanical characteristics of cartilage. Cartilage matrix is degraded and converted to low molecular components mainly by proteases produced by chondrocytes, and these destructive proteases are regulated by inflammatory cytokines and growth factors.

From the Department of Orthopaedic Surgery, Fujita Health University, Second Hospital; Department of Orthopaedic Surgery, Fujita Health University; and Seikagaku Co. Ltd., Tokyo, Japan.

Supported by Seikagaku Co. Ltd.

H. Sugimoto, MD; N. Terada, MD, Associate Professor; S. Kato, MD, Department of Orthopaedic Surgery, Fujita Health University, Second Hospital; H. Yamada, MD, Professor and Chairman; A. Kanaji, MD, Lecturer; H. Date, MD; H. Ichinose, MD, Department of Orthopaedic Surgery, Fujita Health University; K. Miyazaki, Seikagaku Co. Ltd.

Address reprint requests to Prof. H. Yamada, Department of Orthopaedic Surgery, Fujita Health University, Toyoake, Aichi, 470-1192, Japan. E-mail: hayamada@fujita-hu.ac.jp

Accepted for publication July 10, 2006.

Most therapeutic drugs for OA are symptom-modifying drugs that improve the clinical symptoms of OA, such as pain. Few candidate structure-modifying drugs have been confirmed clinically to inhibit cartilage destruction, and the effectiveness of these drugs is currently being investigated in a large-scale clinical study[1,2]. One such drug therapy for OA is intraarticular injection of high molecular weight hyaluronan (HA). HA is a long linear-chain glycosaminoglycan consisting of a repetitive disaccharide unit structure that is the main component of synovial fluid. HA is important in maintaining the viscoelasticity of articular cartilage, and contributes to the maintenance of low friction, which is an important articular function, through synergistic action with cartilage. HA in synovial fluid is produced by synovial cells, and has a molecular weight of about $4–5 \times 10^6$ Da in normal subjects. In arthropathy, such as rheumatoid arthritis and OA, both the molecular weight and concentration of HA are decreased[3]. Such decreases in the molecular weight and concentration of HA impair lubrication between cartilage, decrease impact-absorbing ability, and cause further degeneration of the cartilage. HA receptors, including lymphocyte homing receptors, CD44, are present on the chondrocyte surface. In addition to the hydrody-

namic action described above, HA alters chondrocyte metabolism through receptors, and acts to protect cartilage tissue[4]. HA has been reported to exhibit cartilage-protective effects, including stimulation of chondrocyte proliferation, production of cartilage matrix, inhibition of the production of protease[5], stimulation of the production of a protease inhibitor[6], movement of newly synthesized aggrecan around chondrocyte[7], and inhibition of chondrocyte apoptosis *in vitro* [8].

HA injection improves the clinical symptoms of OA, mainly pain, in about 70% of OA cases, but nonresponders to this therapy do exist. Joint puncture is an invasive procedure that is performed with HA injection. As such, this procedure has a risk of complications, including infection. Prediction of the clinical effectiveness of this therapy enables us to perform efficient medical care.

Measurement of biological markers that are derived from components of joints, such as cartilage, synovial membrane, and bone, in synovial fluid, blood, and urine, has allowed investigation of the pathology of arthropathy[9]. Typical biological markers that reflect cartilage turnover are fragments derived from type II collagen, aggrecan, and other minor proteins that are present in cartilage. Aggrecan-derived markers are core proteins, fragments of aggrecan, glycosaminoglycans (GAG) composing aggrecan, chondroitin 6-sulfate and 4-sulfate (C6S and C4S), and keratan sulfate (KS)[10-12]. Unlike radiograph and magnetic resonance imaging, these biological markers reflect real-time metabolism of joint components, such as cartilage and synovial membrane. Our objective was to investigate the possibility of predicting the effectiveness of HA injection from biological markers in synovial fluid collected at the initiation of intraarticular injection of HA.

MATERIALS AND METHODS

Patients. The subjects were 32 outpatients with OA of the knee (38 joints) at our orthopedic outpatient clinic who had apparent pain on movement and hydrarthrosis, and were indicated for HA injection. No concomitant steroid or nonsteroidal antiinflammatory drugs (NSAID) were administered. Patients treated with HA preparations within the past 3 months and patients with suspected rheumatoid arthritis, trauma, and suppurative arthritis were excluded. The patients' characteristics are shown in Table 1.

Intraarticular injection and collection of synovial fluid. An injection containing 25 mg of HA (molecular weight of about 900,000 Da) in 2.5 ml (superpurified hyaluronate, Seikagaku Co. Ltd., Tokyo, Japan) was injected into the knee joint once a week for one month. Synovial fluid was collected at the initiation of the first injection, and centrifuged at 3000 rpm for 15 minutes at room temperature. The supernatant was collected and immediately stored at -85°C.

Evaluation by radiography. Plain radiograms of the knee (frontal and lateral views and frontal view with weight-bearing) were acquired before the initiation of injection, and the OA stage was determined based on the Koshino classification scale[13] (grade 0: normal, grade 1: osteosclerosis or osteophyte formation, grade 2: narrowing of the joint space to 3 mm or less, grade 3: disappearance of the joint space, grade 4: 5 mm or less bone defect of the weight-bearing surface, grade 5: 5 mm or more bone defect of the weight-bearing surface; Table 1).

Evaluation of clinical symptoms. Clinical evaluation of OA was performed, based on the criteria for judgment of therapeutic results of knee OA established by the Japanese Orthopaedic Association (JOA score)[14]. In this score, pain on walking, pain on ascending and descending the stairs, range of motion, and joint swelling were rated with maximum scores of 30, 25, 35, and 10, respectively. The subjective and objective symptoms were evaluated based on the JOA scores before the initiation of intraarticular injection and at 1 month after injection. Pain was evaluated using the 100 mm visual analog scale (VAS).

Table 1. Patients' characteristics. Stage of knee deformity was assessed by the radiological findings according to the Koshino criteria[13].

	n
Sex	
Male	4
Female	34
Age, yrs	
> 60	4
60–70	5
70–80	10
< 80	19
Radiological stage	(mean = 73.4 ± 8.2)
I	11
II	5
III	13
IV	5
V	4

Measurement of biological markers. C6S and C4S in synovial fluid were measured by high performance liquid chromatography according to the method reported by Shinmei, *et al*[11]. Glycosaminoglycans in synovial fluid were degraded to disaccharides by treatment with chondroitinase ABC and chondroitinase AC-II, and applied to a column packed with propylamine-bound silica gel (YMC gel PA-120; YMC, Kyoto, Japan) for quantification. The aggrecan level was measured using a sandwich ELISA measurement kit (Biosource Co.) This measurement kit uses an anti-KS monoclonal antibody for capturing and a labeled anti-G1-domain monoclonal antibody as a detector, and selectively measures aggrecan molecules with HA-binding ability and a KS side chain[15].

Statistical analysis. The results of measurement of the biological markers were presented as the means ± standard deviation. For analysis of the significance of between-group differences, paired t test or Wilcoxon signed-rank test was used. For analysis of correlation, Spearman's correlation coefficient by rank was used (StatView 5.0, Abacus Concepts Inc., Berkeley, CA, USA).

RESULTS

Time-course of changes in biological markers after injection. The C6S and C4S concentrations in synovial fluid showed no significant change after injection for 1 month. C6S/C4S and aggrecan concentration decreased over time, but the decrease was not significant (Figure 1).

Relationship between biological markers before injection and improvement of clinical symptoms. The relationships between the concentrations of the biological markers before HA injection and improvement of the JOA score and VAS one month after initiation of injection were investigated by regression analysis.

A significant positive correlation was observed between the C6S concentration before injection and improvement of the JOA score after one month ($r = 0.322$, $p = 0.0383$; Figure 2). No significant correlation was apparent between the C4S

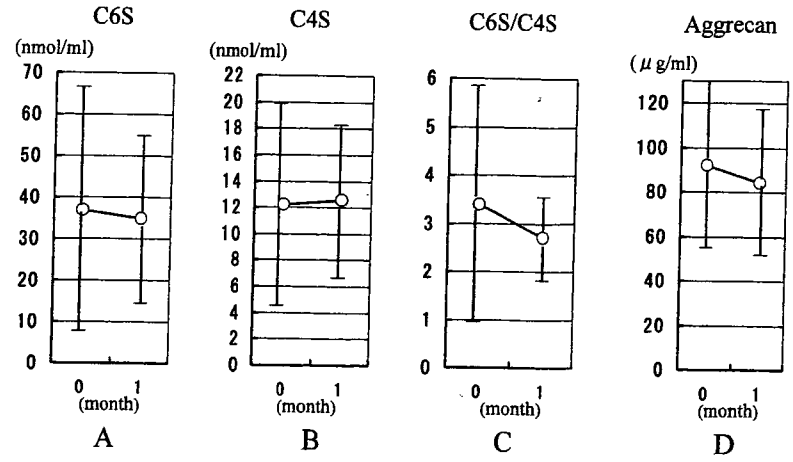

Figure 1. Time-course of changes in biological markers. HA with MW 800,000 Da was injected into the knee joint once a week for one month. C6S and C4S in synovial fluid were measured by HPLC. The aggrecan level in synovial fluid was measured using a sandwich ELISA measurement kit. Data were shown as mean ± SD. A: C6S. B: C4S. C: C6S/C4S. D: Aggrecan.

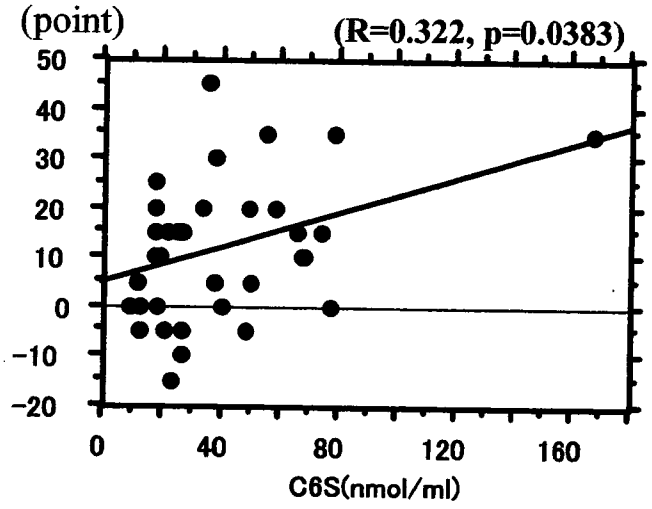

Figure 2. Relationship between C6S concentration before injection and improvement of JOA score. The relationships between C6S concentration before HA injection and improvement of the JOA score one month after initiation of injection were investigated by regression analysis.

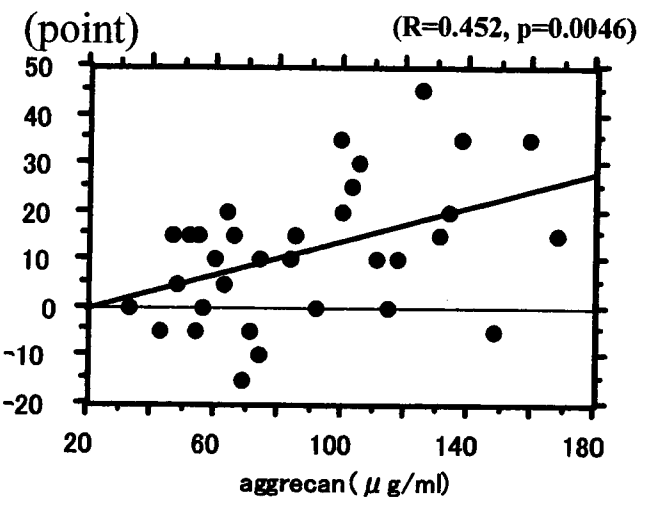

Figure 3. Relationship between aggrecan concentration before injection and improvement of JOA score. The relationships between aggrecan concentration before HA injection and improvement of the JOA score one month after initiation of injection were investigated by regression analysis.

concentration or C6S/C4S before injection and the improvement of the JOA score (data not shown). A significant correlation was observed between the aggrecan concentration before injection and improvement of the JOA score after 1 month ($r = 0.452$, $p = 0.0046$; Figure 3). In contrast, no significant correlation was apparent between the biological marker concentrations before injection and improvement of VAS (data not shown). Relationship between level of biological marker and improvement of each item of JOA score was analyzed. Significant correlation was observed between C6S concentration before injection and improvement of pain on waking ($r = 0.465$, $p = 0.0221$), and range of motion ($r = 0.433$, $p = 0.0282$) after one month. Aggrecan concentration correlated significantly with improvement of pain on walking ($r = 0.451$, $p = 0.0268$), and pain on ascending and descending the stairs ($r = 0.577$, $p = 0.0025$) after one month. OA stage determined by radiographic findings had no significant relation with improvement of both the JOA score and VAS (Figure 4).

DISCUSSION

In OA, viscoelastic substances in synovial fluid, mainly HA, become deteriorated. Intraarticular injection of HA has been initiated based on the concept of viscosupplementation: supplementation of deteriorated HA with a novel viscoelastic substance that exhibits a hydrodynamic function[16]. HA has

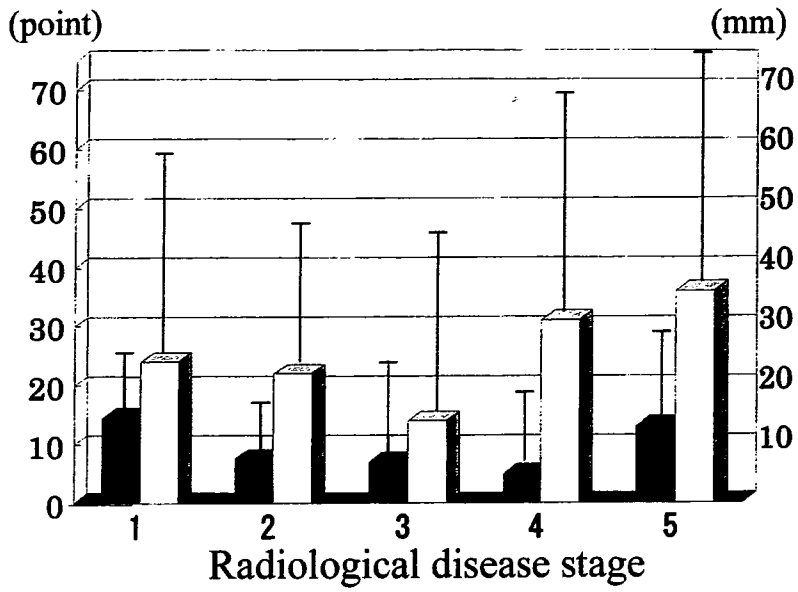

Figure 4. Radiological disease stage and improvement of JOA score and VAS. OA disease stage determined by radiographic findings had no significant relation with improvement both of the JOA score and VAS. Data were shown as mean ± SD. Black bar: JOA score (points). White bar: VAS (mm).

been considered as a symptom-modifying drug that primarily improves the pain of OA[17]. HA injection apparently improved the clinical symptoms of OA, including pain, in this study.

Cartilage markers are divided into markers of synthesis and catabolism. Typical markers of catabolism reflecting the destruction of cartilage include aggrecan molecules released from aggrecan, side chain KS, and CS. There are 2 types of CS: C6S, which is abundant in healthy cartilage, and C4S, which is abundant in degenerated cartilage as with OA[18]. Changes in joint markers during the course of treatment of OA can help in determining the effectiveness of treatment. Yamada, *et al* measured various joint markers in synovial fluid before and after HA injection into the joint in patients with knee OA, and found that the PIICP concentration increased significantly after HA injection[19]. Since PIICP is a marker of the synthesis of type II collagen[20,21], this finding suggested that HA injection promoted matrix synthesis by chondrocytes. In studies reported by Namiki, *et al*, and Uesaka, *et al*[22,23], C6S and C4S levels decreased after HA injection. In our study, aggrecan level was decreased after injection of HA for one month, but this decrease was not significant. Thus, our study did not demonstrate inhibition of the degradation of cartilage aggrecan by HA injection in OA.

There has been no report of prediction of the efficacy of intraarticular injection of HA for OA based upon biological markers. We observed a significant positive correlation between the C6S concentration before injection and improvement of the JOA score after one month of injection. Furthermore, a stronger positive correlation, compared with that of C6S, was noted between the aggrecan concentration before injection and the JOA score after one month of injection. However, radiological OA stage had no significant relation with improvement both of the JOA score and VAS. These findings suggest that improvement of the clinical symptoms after initiation of HA injection can be predicted by measurement of the fragments derived from aggrecan. Yamada, *et al* reported that the concentration of aggrecan fragments in synovial fluid decreased with the progression of OA, as a result of decreases in the amount of residual cartilage and suppression of chondrocyte metabolism with the advancement of OA[24-26]. In consideration of these observations, our findings indicate that HA injection is effective for cases with a high intraarticular level of aggrecan fragments. This reflects an early stage of OA in keeping with residual cartilage and chondrocyte metabolic activity.

REFERENCES

1. Reginster JY, Deroisy R, Rovati LC, et al. Long-term effects of glucosamine sulphate on osteoarthritis progression: a randomized, placebo-controlled clinical trial. Lancet 2001;357:251-6.
2. Richy F, Bruyere O, Ethgen O, Cucherat M, Henrotin Y, Reginster JY. Structural and symptomatic efficacy of glucosamine and chondroitin in knee osteoarthritis: a comprehensive meta-analysis. Arch Intern Med 2003;163:1514-22.
3. Dahl LB, Dahl IMS, Engstrom LA. Concentration and molecular weight of sodium hyaluronate in synovial fluid from patients with rheumatoid arthritis and other arthropathies. Ann Rheum Dis 1985;44:817-22.
4. Lisignoli G, Grassi F, Zini N, et al. Anti-Fas-induced apoptosis in chondrocytes reduced by hyaluronan: evidence for CD44 and CD54 (intercellular adhesion molecule 1) involvement. Arthritis Rheum 2001;44:1800-7.
5. Kikuchi T, Shinmei M. Effects of hyaluronan on proteoglycan metabolism of rabbit articular chondrocytes in cultures. Jpn J Rheumatol 1994;5:207-15.

6. Yasui T, Akatsuka M, Tobetto K, et al. Effects of hyaluronan on the production of stromelysin and tissue inhibitor of metalloproteinase-1 (TIMP-1) in bovine articular chondrocytes. Biomed Res 1992;13:343-8.
7. Kikuchi T, Yamada H, Fujikawa K. Effects of high molecular weight hyaluronan on the distribution and movement of proteoglycan around chondrocytes cultured in alginate beads. Osteoarthritis Cartilage 2001;9:351-6.
8. Takahashi K, Hashimoto S, Kubo T, Hirasawa Y, Lotz M, Amiel D. Effect of hyaluronan on chondrocyte apoptosis and nitric oxide production in experimentally induced osteoarthritis. J Rheumatol 2000;27:1713-21.
9. Garnero P, Rousseau JC, Delmas PD. Molecular basis and clinical use of biochemical markers on bone, cartilage, and synovium in joint diseases. Arthritis Rheum 2000;43:953-68.
10. Campion GV, McCrae F, Schnitzer TJ, Lenz ME, Dieppe PA, Thonar EJ-MA. Levels of keratan sulfate in the serum and synovial fluid of patients with osteoarthritis of the knee. Arthritis Rheum 1991;34:1254-9.
11. Shinmei M, Miyauchi S, Machida A, Miyazaki K. Quantitation of chondroitin 4-sulfate and chondroitin 6-sulfate in pathologic joint fluid. Arthritis Rheum 1992;35:1304-8.
12. Lohmander LS, Hoerrner LA, Lark MW. Metalloproteinases, tissue inhibitor, and proteoglycan fragments in knee synovial fluid in human osteoarthritis. Arthritis Rheum 1993;36:181-9.
13. Koshino T. Etiology, classifications and clinical findings of osteoarthritis of the knee [Japanese]. Ryumachi 1985;25:191-203.
14. The Japanese Orthopaedic Association Japanese Knee Society. Assessment criteria for knee diseases and treatments. Tokyo: Kanehara, 1994.
15. Guerne PA, Desgeorges A, Jaspar JM, et al. Effects of IL-6 and its soluble receptor on proteoglycan synthesis and NO release by human articular chondrocytes: comparison with IL-1. Modulation by dexamethasone. Matrix Biology 1999;18:253-60.
16. Peyron JG, Balazs LA. Preliminary clinical assessment of Na-hyaluronate injection into human arthritic joints. Pathol Biol 1974;22:731-6.
17. Altman RD. Intra-articular sodium hyaluronate in osteoarthritis of the knee. Semin Arthritis Rheum 2000;30:11-8.
18. Mankin HJ, Lippello L. The glycosaminoglycans of normal and arthritic cartilage. J Clin Invest 1971;50:1712-9.
19. Yamada H, Yoshihara Y, Kobayashi T, et al. Intra-articular injection therapy with high-molecular weight hyaluronan for osteoarthritis of the knee joint—Effects on joint fluid markers. Orthopaedics International Edition 1997;5:117-21.
20. Shinmei M, Ito K, Matsuyama S, Yoshihara Y, Matsuzawa K. Joint fluid carboxy-terminal type II procollagen peptide as a marker of cartilage collagen biosynthesis. Osteoarthritis Cartilage 1993;1:121-8.
21. Sugiyama S, Itokazu M, Suzuki Y, Shimizu K. Procollagen II C propeptide level in the synovial fluid as a predictor of radiographic progression in early knee osteoarthritis. Ann Rheum Dis 2003;62:27-32.
22. Namiki O, Kuriyama S, Maeda H, Sakamoto A. Biochemical analysis of synovial fluid and their alteration in intra-articular injection therapy of sodium hyaluronate in osteoarthritis. Joint Surgery 1994; 21:131-7.
23. Uesaka S, Takeuchi T, Ide K, Yoshihara K, Nakayama Y, Shirai Y. Intra-articular injection therapy with sodium hyaluronate for osteoarthritis of the knee—Correlation between radiographic prognosis of osteoarthritis, joint markers and clinical evaluations. Joint Surgery 1999;26:106-12.
24. Yamada H, Miyauchi S, Hotta H, et al. Levels of chondroitin sulfate isomers in the synovial fluids from patients with hip osteoarthritis. J Orthop Science 1999;4:250-4.
25. Yamada H, Miyauchi S, Morita M, et al. Content and sulfation pattern of keratan sulfate in hip osteoarthritis using high performance liquid chromatography. J Rheumatol 2000;27:1721-4.
26. Kato S, Yamada H, Terada N, et al. Joint biomarkers in idiopathic femoral head osteonecrosis: comparison with hip osteoarthritis. J Rheumatol 2005;32:1518-23.

J|A|C|S
COMMUNICATIONS

Published on Web 04/12/2006

Semipermeable Polymer Vesicle (PICsome) Self-Assembled in Aqueous Medium from a Pair of Oppositely Charged Block Copolymers: Physiologically Stable Micro-/Nanocontainers of Water-Soluble Macromolecules

Aya Koide,[†] Akihiro Kishimura,[†,‡,§] Kensuke Osada,[†,§] Woo-Dong Jang,[†,‡,∥] Yuichi Yamasaki,[†,‡,§] and Kazunori Kataoka*[,†,‡,§]

Department of Materials Engineering, Graduate School of Engineering, and Center for NanoBio Integration, The University of Tokyo, 7-3-1 Hongo, Bunkyo-ku, Tokyo 113-8656 Japan, and CREST, Japan Science and Technology Agency, Japan

Received November 24, 2005; E-mail: kataoka@bmw.t.u-tokyo.ac.jp

Polymer vesicles enclosing a volume with a molecularly thin membrane, known as "polymersomes", have recently been attracting progressive attention from both fundamental and applied standpoints as carriers or containers for various functionality compounds.[1,2] Particularly, in an aqueous entity, amphiphilic block copolymers have been used for the preparation of polymersomes,[1-3] revealing unique characteristics such as high structural stability compared to conventional liposomes made from low molecular amphiphiles.[1] Very recently, stable encapsulation of biologically relevant substances, including drugs and enzymes, into the polymersomes has been directed to applications as delivery and bioreactor systems.[2] Nevertheless, the hydrophobic nature of the membrane in such amphiphilic polymersomes prevents the penetration of hydrophilic solutes, limiting their functionality as semipermeable container systems. Furthermore, the harsh preparation conditions, including the use of organic solvents, may hamper the encapsulation of fragile compounds such as proteins. Herein, we report for the first time the preparation of stable polymersomes with a semipermeable membrane through a simple mixing of a pair of oppositely charged block copolymers in an aqueous medium. The polymersome formed in this way is a new entity of polymer vesicles with a polyion complex (PIC) membrane and thus may be given a new terminology as a "PICsome".

A PICsome as a hollow sphere needs the formation of a stable layer of PIC lamellae as the partition membrane. In this regard, oppositely charged segments of the block copolymer pair are preferred to have a matched chain length, compensating for the counter charge in a stoichiometric manner and minimizing the phase mixing of the PIC middle layer with the outer and inner shell layers of the hydrophilic segment, in this case, poly(ethylene glycol) (PEG). Here, to satisfy this condition of matched chain length, both anionic and cationic block copolymers were prepared from the same platform polymer, PEG-poly(β-benzyl-L-aspartate) (PEG-PBLA), to have identical molecular weight and composition (Scheme 1). Two types of PEG-PBLA with a different PBLA composition (degree of polymerization (DP) of PBLA; 17 and 100) were prepared by the ring opening polymerization of β-benzyl-L-aspartate *N*-carboxyanhydride initiated from the ω-primary amino group of $CH_3O-PEG-NH_2$ (M_n = 2000, M_w/M_n = 1.05).[4] The anionic component of the PICsome, PEG-poly(α,β-aspartic acid) (PEG-P(Asp)$_{17}$ and PEG-P(Asp)$_{100}$), was obtained from PEG-PBLA by alkali hydrolysis as reported previously.[5] Alternatively, the cationic

Scheme 1. Synthesis of a Pair of Oppositely Charged Block Copolymers

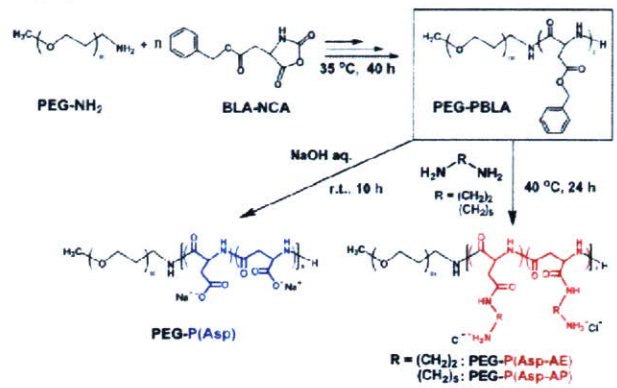

component was prepared from PEG-PBLA by aminolysis of flanking benzyl ester groups with an excess amount of diamine. A notable property of PBLA is that the benzyl ester groups can easily undergo quantitative aminolysis reactions with various diamines at ambient temperature via the formation of a succinimidyl ring structure as an intermediate, allowing the preparation of cationic poly(aspartamide)s with different amine functionalities. Indeed, quantitative aminolysis was confirmed from ^{1}H NMR spectra.[4] Two types of diamines with a different number of methylene units, 1,2-diaminoethane and 1,5-diaminopentane, were used in the aminolysis to obtain PEG-poly([2-aminoethyl]-α,β-aspartamide) (PEG-P(Asp-AE)$_{17}$ and PEG-P(Asp-AE)$_{100}$) and PEG-poly([5-aminopentyl]-α,β-aspartamide) (PEG-P(Asp-AP)$_{17}$ and PEG-P(Asp-AP)$_{100}$), respectively, to explore the effect of the alkyl-spacer length on the self-assembly behavior.

The anionic and cationic block copolymers were separately dissolved in 10 mM Tris-HCl buffer (pH 7.4) with a physiological salt concentration of 150 mM NaCl. Both solutions were then mixed in an equal ratio of $-COO^-$ and $-NH_3^+$ units to form PIC and subsequently subjected to sonication.[4] Flow particle image analysis[4] and dark-field microscopic (DFM) observation suggested the formation of spherical particles with the diameter up to 10 μm in the PEG-P(Asp)$_{100}$/PEG-P(Asp-AP)$_{100}$ system (Figure 1), which is obviously with a larger size range than that of the well-documented PIC micelles with a core−shell architecture.[6] The DFM image was more fascinating, showing characteristic ringlike scatterings (Figure 1), suggesting the hollow structure of the particles. Note that the scattering light intensity in DFM correlates with the density of the objects, giving a ringlike image for hollow particles with a large density difference between the inner and peripheral regions.[7] The

† Department of Materials Engineering, Graduate School of Engineering, The University of Tokyo.
‡ CREST, Japan Science and Technology Agency.
§ Center for NanoBio Integration, The University of Tokyo.
∥ Present address: Department of Chemistry, Yonsei University, Korea.

10.1021/ja057993r CCC: $33.50

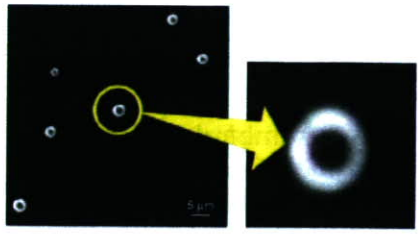

Figure 1. Dark-field microscopic images of PICsomes prepared from a PEG-P(Asp)$_{100}$/PEG-P(Asp-AP)$_{100}$ system.

balance of the segment length in the block copolymer is expected to play a substantial role in the self-assembly process. Indeed, the combination of the block copolymers with a shorter charged segment, PEG-P(Asp)$_{17}$/PEG-P(Asp-AP)$_{17}$ system, gave a DFM image with only few ring-scattering objects dispersed in the major part of the small dot scatterings presumably from micelles. Block copolymers with shorter charged segments compared to the PEG segment adopt a cone-shaped conformation preferring the micelle architecture.[6] The molecular shape gradually changes from cone to rod with the increased length of the charged segments relative to the PEG segments, and eventually, the assembly should adopt the vesicular structure with a smaller curvature than the spherical micelle.[8] The observations here are consistent with this general rule of vesicular formation through molecular assembly. Another factor influencing the vesicular formation seems to be the alkyl-spacer length of the cationic side chain of the poly(aspartamide) segment, which may be related to the flexibility of the ion pair formed in the PIC structure. A decrease in the alkyl-spacer length from pentyl to ethyl in the side chain of the cationic poly(aspartamide) segment, viz. the PEG-P(Asp)$_{100}$/PEG-P(Asp-AE)$_{100}$ system, resulted in a significant decrease in the size (<1 μm) of the ring scatterings observed in DFM. It is likely that the length of the alkyl spacer may be a critical factor in determining the stable PICsome size, yet a further detailed study should be needed to confirm this assumption.

The hollow structure of the large PIC assembly from PEG-P(Asp)$_{100}$/PEG-P(Asp-AP)$_{100}$ system as "PICsome" was further directly evidenced from the encapsulation of the water-soluble macromolecule labeled with fluorescein isothiocyanate, FITC-dextran (FITC-Dex, M_n = 40 000), into the PICsome. Cross-sectional observation by the confocal laser scanning microscope (CLSM) clearly confirmed the successful inclusion of FITC-Dex into the PICsome by a simple mixing of PEG-P(Asp-AP)$_{100}$ (1 mg/mL) with PEG-P(Asp)$_{100}$ (1 mg/mL) containing FITC-Dex (1 mg/mL) (Figure 2).[4] The PICsome with encapsulating FITC-Dex was appreciably stable in physiological buffer as observed by CLSM even after 3 months standing at ambient temperature.

The semipermeability of the PICsome membrane was then investigated using fluorescent molecules with different molecular weights. The fluorescence collected through the objective lens was resolved by the diffraction grating and monitored by a 32-channel arrayed detector. Upon addition of dextran labeled with tetramethylrhodamine isothiocyanate (TRITC-Dex, M_n = 70 000) to the solution of PICsome with encapsulated FITC-Dex, a green fluorescence of FITC inside the PICsome was clearly observed, sharply discriminated from the red fluorescence of TRITC-Dex in the outer medium, in the merged image of CLSM taken at the excitation wavelength for FITC and TRITC (488 and 543 nm) (Figure 2a). On the other hand, upon addition of free TRITC (MW = 443.5) to the solution of the FITC-Dex encapsulating PICsome, a yellow color was observed inside the PICsome (Figure 2b).[4] An emission spectrum of the region of interest (ROI) in Figure 2b shows the

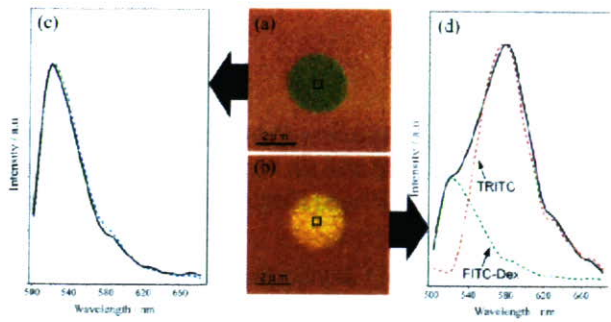

Figure 2. CLSM images and emission spectra of PICsome encapsulating FITC-Dex. Images after the addition of (a) TRITC-Dex or (b) TRITC. (c) Spectra of the ROI in (a) after (solid line) and before (blue dotted line) the addition of TRITC-Dex. (d) A spectrum of the ROI in (b) (solid line) with reference spectra of FITC-Dex (green dotted line) and TRITC (red dotted line).

intense fluorescence with the maximum at 580 nm and the shoulder at 520 nm (Figure 2d). The profile was reasonably fitted with both references of FITC-Dex and TRITC, indicating the penetration of TRITC into the PICsome interior. In contrast, the spectrum of the ROI in Figure 2a corresponds to the spectrum of FITC-Dex before the addition of TRITC-Dex (Figure 2c), indicating the segregation of TRITC-Dex from the PICsome interior. These results visually demonstrated the semipermeable character of the PIC membrane. Notably, the PICsome was able to retain its vesicular structure in the presence of a colloidal osmotic pressure of approximately 10 μOsm from the encapsulated FITC-Dex and was stable even in the medium containing 10% fetal bovine serum at 37 °C,[4] being feasible for biomedical applications.

In summary, a novel entity of a polymer vesicle, a PICsome, was prepared here by a simple mixing of a pair of oppositely charged block copolymers composed of biocompatible PEG and poly(amino acid)s in an aqueous medium. The PICsome is stable in proteinous medium and has a partition membrane with a unique three-layered structure. These biocompatible composition and biologically relevant characteristics of the PICsomes may open their future utility in biomedical fields such as carriers of therapeutic compounds and compartments for diagnostic enzymes.

Acknowledgment. We thank Prof. K. Akiyoshi and Dr. S. M. Nomura (Tokyo Medical and Dental University) for valuable suggestions for DFM observation and Mr. F. Ishidate (Carl Zeiss Co., Ltd.) for emission spectrum measurements.

Supporting Information Available: Syntheses, characterizations, and preparations of PICsomes. This material is available free of charge via the Internet at http://pubs.acs.org.

References

(1) (a) Discher, D. E.; Eisenberg, A. *Science* **2002**, *297*, 967−973. (b) Geng, Y.; Ahmed, F.; Bhasin, N.; Discher, D. E. *J. Phys. Chem. B* **2005**, *109*, 3772−3779. (c) Antonietti, M.; Förster, S. *Adv. Mater.* **2003**, *15*, 1323−1333.
(2) Brož, P.; Benito, S. M.; Saw, C.-L.; Burger, P.; Heider, H.; Pfisterer, M.; Marsch, S.; Meier, W.; Hunziker, P. *J. Control. Release* **2005**, *102*, 475−488. (b) Ranquin, A.; Versées, W.; Meier, W.; Steyaert, J.; Van Gelder, P. *Nano Lett.* **2005**, *5*, 2220−2224.
(3) (a) Bellomo, E. G.; Wyrsta, M. D.; Pakstis, L.; Pochan, D. J.; Deming, T. J. *Nat. Mater.* **2004**, *3*, 244−248. (b) Rodoríguez-Hernández, J.; Lecommandoux, S. *J. Am. Chem. Soc.* **2005**, *127*, 2026−2027.
(4) See Supporting Information.
(5) Yokoyama, M.; Inoue, S.; Kataoka, K.; Yui N.; Okano, T.; Sakurai, Y. *Makromol. Chem.* **1989**, *190*, 2041−2054.
(6) (a) Harada, A.; Kataoka, K. *Macromolecules* **1995**, *28*, 5294−5299. (b) Harada, A.; Kataoka, K. *Science* **1999**, *283*, 65−67. (c) Kataoka, K.; Harada, A.; Nagasaki, Y. *Adv. Drug Delivery Rev.* **2001**, *47*, 113−131.
(7) Hotani, H. *J. Mol. Biol.* **1984**, *178*, 113−120.
(8) Zhang, L.; Eisenberg, A. *J. Am. Chem. Soc.* **1996**, *118*, 3168−3181.

JA057993R